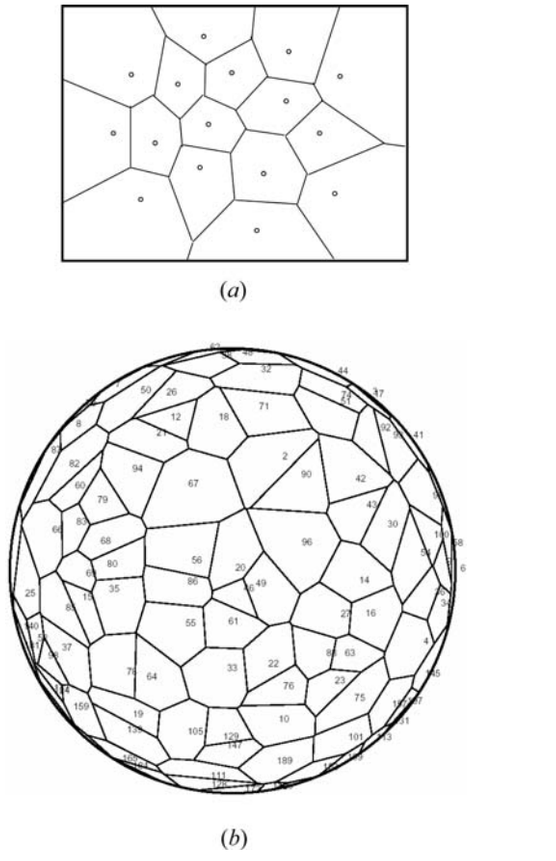

Fig. 2.5.6.7. Partitions of the sampling Fourier space using Voronoi diagrams in direct inversion algorithms. (*a*) Central section of a 3D Fourier volume with sampling points originating from 2D Fourier transforms of projections. Although 2D projections are sampled on a uniform (Cartesian) grid, the arbitrary rotations of projections in 3D space yields a nonuniform distribution of points in three dimensions. In effect, the 3D reconstruction by direct inversion using 3D FFT is not possible. (*b*) Voronoi diagram on a sphere in the GDFR algorithm. Using the reverse gridding method, the 2D Fourier transforms of projections are resampled onto 1D central lines using a constant angular step. In 3D Fourier space, they are located on central sections and their angular directions are evenly distributed on grand circles. However, since central sections have nonuniform distributions, the distribution of angular directions (sampling points on the unitary sphere) is also nonuniform and effectively random.

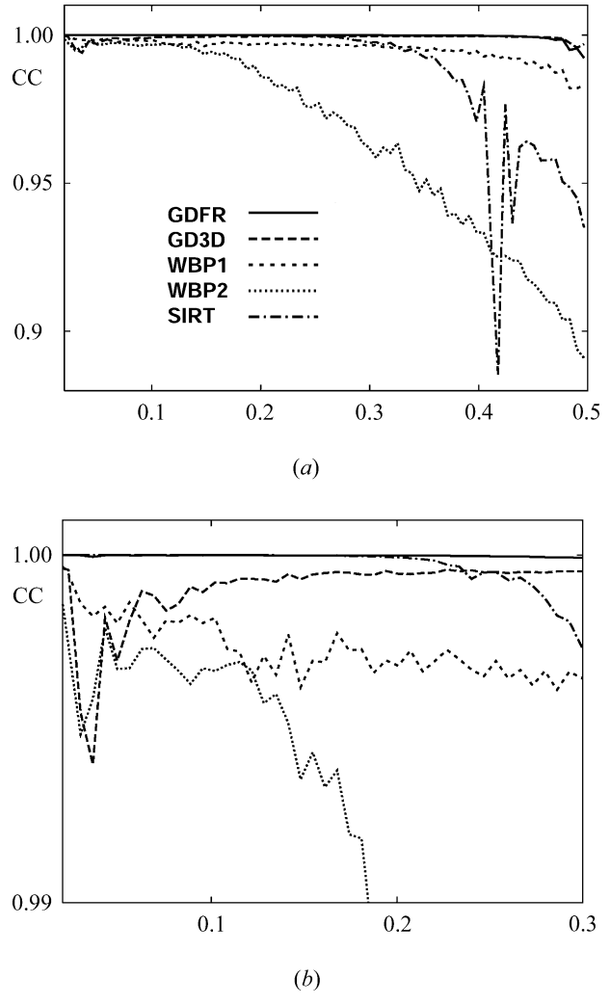

Fig. 2.5.6.8. (*a*) Plot of correlation coefficients (CCs) calculated between Fourier transforms of the reconstructed structure and the original phantom as a function of the magnitude of the spatial frequency using five reconstruction algorithms. GDFR: gridding direct Fourier reconstruction with Voronoi weights; GD3D: gridding reconstruction with simplified gridding weights; WBP1: general weighted backprojection with exponent-based weighting function; WBP2: exact filter weighted backprojection; SIRT: simultaneous iterative reconstruction algorithm. Noise-free projection data were computed in Fourier space using the reverse gridding method. (*b*) Rescaled version of the low-frequency range of (*a*). Note the different scales in (*a*) and (*b*). The horizontal axis is scaled in absolute frequency units with 0.5 equal to the Nyquist frequency.

Note the reverse gridding does not require explicit gridding weights, as in the third step they are constant (Penczek *et al.*, 2004).

In GDFR, the third step of the reversed gridding results in a set of 1D Fourier central lines $\mathcal{F}[\varphi_{1l}]$ calculated using a constant angular step. Clearly, upon inverse Fourier transform they amount to a Radon transform $\varphi_1(u, \psi)$ of the projection and, upon repeating the process for all available projections, they yield a Radon transform $\varphi_1(u, \boldsymbol{\theta})$ of a 3D object φ_3 (albeit non-uniformly sampled with respect to Eulerian angles). Thus GDFR, in addition to being a method of inverting a 3D ray transform, is also a highly accurate method of inverting a 3D Radon transform. GDFR is implemented in the *SPIDER* package (Frank *et al.*, 1996).

The results of a comparison of selected reconstruction algorithms are shown in Fig. 2.5.6.8. The tests were performed using simulated data with the projections of a phantom 3D structure calculated using the inverse gridding method (Penczek *et al.*, 2004). The GDFR yields a virtually perfect reconstruction that agrees with the phantom over the whole frequency range (with the exception of the highest frequencies, but these cannot be reproduced due to geometrical limitations). GD3D is also a gridding-based reconstruction algorithm, in which the gridding weights are calculated directly from contributions of the weighting function to the 3D Fourier pixels and are applied to the voxels in the 3D Fourier volume (Jackson *et al.*, 1991). This yields an approximation to the 'local density' of contributing projections. The simplified gridding weights in GD3D result in deterioration of the reconstruction in the low- and intermediate-frequency ranges. The general weighted backprojection with exponent-based weighting function (WBP1) performs quite well, although reproduction in the low-frequency range is inferior. Similar artifacts are present in the reconstruction using the exact filter weighted backprojection (WBP2), which, in addition, performs disappointingly at higher frequencies. This relatively poor performance is attributed to the nonoptimal weighting schemes used in both methods. It is also interesting to note that the backprojection step is identical in both algorithms; they only differ by the weighting function. The significant difference in their performance attests to the importance of good weighting schemes for high-quality 3D reconstructions from nonuniformly distributed projections. SIRT yields a reconstruction that in the low- and intermediate-frequency ranges matches in quality the reconstruction obtained with GDFR. However, there is a significant loss of quality at high frequencies. This is due to the